Theor Chem Acc (2002) 107:117–129
DOI 10.1007/s00214-001-0315-9

Theoretical
Chemistry Accounts

Feature article

Orbital-band interactions and the reactivity of molecules on oxide surfaces: from explanations to predictions

José A. Rodriguez

Department of Chemistry, Brookhaven National Laboratory, Upton, NY 11973, USA
e-mail: rodrigez@bnl.gov

Received: 21 June 2001 / Accepted: 8 October 2001 / Published online: 1 February 2002
© Springer-Verlag 2002

Abstract. The surface chemistry of oxides is relevant for many technological applications: catalysis, photoelectrolysis, electronic-device fabrication, prevention of corrosion, sensor development, etc. This article reviews recent theoretical works that deal with the surface chemistry of oxides. The account begins with a discussion of results for the adsorption of CO and NO on oxides, systems which have been extensively studied in the literature and constitute an ideal benchmark for testing the quality of different levels of theory. Then, systematic studies concerned with the behavior of adsorbied alkali metals and sulfur-containing molecules are presented. Finally, a correlation between the electronic and chemical properties of mixed-metal oxides is analyzed and basic principles for designing chemically active oxides are introduced. Advances in theoretical methods and computer capabilities have made possible a fundamental understanding of many phenomena associated with the chemistry of molecules on oxide surfaces. Still many problems in this area remain as a challenge, and the approximate nature of most theoretical methods makes necessary a close coupling between theory and experiment. Following this multidisciplinary approach, the importance of band-orbital interactions for the reactivity of oxide surfaces has become clear. Simple models based on band-orbital mixing can explain trends found for the interaction of many adsorbates with oxide surfaces. These simple models provide a conceptual framework for modifying or controlling the chemical activity of pure oxides and for engineering mixed-metal oxides. In this respect, theoretical calculations can be very useful for predicting the best ways for enhancing the reactivity of oxide systems and reducing the waste of time, energy and materials characteristic of an empirical design.

Key words: Oxides – Density functional calculations – Adsorption – Catalysis

1 Introduction

The metal elements are able to form a large diversity of oxide compounds. These oxides adopt a vast number of structural geometries and at an electronic level they can exhibit metallic character or behave as semiconductors or insulators [1, 2]. The surface chemistry of oxides is relevant for many technological applications [1, 3]: catalysis, photoelectrolysis, electronic-device fabrication, prevention of corrosion, sensor development, etc. From a practical viewpoint, one of the most important applications of oxides is in the area of catalysis [1, 3, 4]. In the chemical and petrochemical industries, products worth billions of dollars are generated every year through processes that use oxide and metal/oxide catalysts [3, 4]. In the control of environmental pollution, catalysts or sorbents that contain oxides are employed to remove the CO, NO_x and SO_x species formed during the combustion of fossil-derived fuels [3–6]. Furthermore, the most active areas of the semiconductor industry involve the use of oxides [7], and in many cases gas-oxide reactions play a predominant role in the fabrication or performance of electronic devices.

Obtaining fundamental knowledge of the factors that control the chemical properties of oxide surfaces is a challenge for modern science and a prerequisite for the rational design of catalysts and other technological devices. Many of these systems are very complex in nature [3, 4, 7]. In principle, when a molecule adsorbs on an oxide surface it can interact with the oxygen and/or metal centers of the substrate. For oxides, it is known that the chemical properties of the metal centers usually depend on the number of oxygen vacancies around them [1, 3]. In addition, there can be big variations in chemical reactivity when changing from one oxide substrate to another [1, 8, 9]. Thus, the main objective is to under-

stand how the structural and electronic properties of a surface affect the energetics for adsorption processes and the paths for dissociation and chemical reactions. Since metal oxides are ionic compounds, the strength of the bond of a molecule with an oxide surface depends on the extent of band-orbital mixing and electrostatic interactions between the charge distribution in the adsorbate and the Madelung field of the oxide [1, 8, 9]. In recent years, advances in instrumentation and experimental procedures have allowed a large series of novel works on the surface chemistry of oxides [1, 8, 10–14]. In many cases, these experimental studies have shown interesting and unique phenomena. Theory is needed to unravel the basic interactions behind these phenomena and to provide a general framework for the interpretation of experimental results [1, 14]. Ideally, using theoretical methods, one should be able to predict patterns in the chemical reactivity of oxide surfaces [15–18].

As in the case of experimental techniques, no single theoretical approach is able to address the large diversity of phenomena occurring on oxide surfaces [1, 15–17]. Oxide surfaces are usually modeled using either a finite cluster embedded in a large array of point charges or a two-dimensional periodic slab [1, 15, 19, 20]. Many articles have been published comparing the results of these two approaches [15, 19–24]. An important advantage of the cluster approach is that one can use the whole spectrum of quantum-chemical methods developed for small molecules with relatively minor modifications. On the other hand, the numerical effort involved in cluster calculations increases rather quickly with the size of the cluster, and for many oxides systems a priori it is not clear how to choose the magnitude of the point charges surrounding the cluster to mimic the effects of the Madelung field [15, 20]. This problem does not exist when using slab models. Owing to the explicit incorporation of the periodicity of the crystal lattice through the Bloch theorem, the actual dimension of a slab calculation depends only on the size of the unit cell [15, 25]. In practical terms, the slab approach is mainly useful for investigating the behavior of adsorbates at medium and high coverages. Very large unit cells are required at the limit of low to zero coverage or when examining the properties and chemical behavior of isolated defect sites in an oxide surface. In these cases, from a computational viewpoint, the cluster approach can be much more cost effective than the slab approach. Slab and cluster calculations can be performed at different levels of sophistication: semiempirical methods, simple ab initio Hartree–Fock (HF), ab initio post-HF (configuration interaction, second-order Møller–Plesset, etc.), and density functional (DF) theory [1, 15–18, 26, 27]. DF-based calculations frequently give adsorption geometries with a high degree of accuracy and predict reliable trends for the energetics of adsorption reactions [17, 18].

This article provides a review of recent theoretical works that deal with the surface chemistry of oxides. A significant fraction of the account is focused on the importance of orbital-band interactions in bonding and how they determine the reactivity of oxide surfaces. The account begins with a discussion of results for the adsorption of CO and NO on oxides, systems which have been extensively studied in the literature and constitute an ideal benchmark for testing the quality of different levels of theory. Then, systematic studies concerned with the behavior of adsorbed alkali metals and sulfur-containing molecules are presented. Finally, a correlation between the electronic and chemical properties of mixed-metal oxides is analyzed and fundamental principles for engineering chemically active oxides are introduced. It is shown that theoretical methods have evolved to the point that they are not only useful for explaining experimental data, but also have predictive power.

2 Adsorption of CO and NO on oxides

In this section, we examine in detail the bonding of CO and NO to MgO(100) and TiO_2(110) (Fig. 1). These two substrates are probably the most studied oxide surfaces in the literature [19, 20, 23, 28–30]. Powders of these oxides are used in many industrial applications owing to their low cost [3–5]. The calculated (DF-generalized gradient approximation, GGA) energy positions for the valence and conduction bands of bulk MgO and TiO_2 [31] are displayed in Fig. 2. For MgO, the calculations predict a band gap of about 5 eV. Experimental measurements give band gaps of 6–6.5 eV, depending on the techniques employed [1, 22]. The band gap predicted for TiO_2 (about 1.5 eV) is also smaller than the

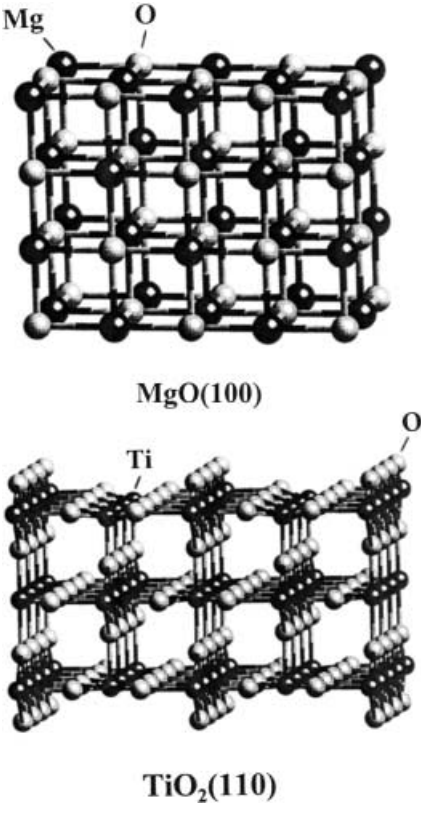

Fig. 1. Schematic representation for the MgO(100) and TiO_2(110) surfaces. In the case of MgO(100), the surface (top layer) and three layers underneath are shown. For TiO_2(110), the diagram shows the surface (top layer) and two layers underneath

corresponding value obtained experimentally (about 3 eV [1]); however, the DF calculations reproduce well the experimental trend ($MgO > TiO_2$). In the case of MgO, several theoretical studies indicate that the compound is almost fully ionic [19, 22, 32, 33]. On the other hand, the Ti–O bonds have a large degree of covalent character and TiO_2 is best described as an ionocovalent oxide [20, 34, 35]. Since MgO and TiO_2 exhibit pronounced differences in their electronic properties, they are ideal for examining the relative importance of several phenomena frequently associated with the bonding of molecules to oxides [19, 20]: band-orbital hybridizations and subsequent electron transfer between adsorbate and surface, effects of Pauli repulsion, charge polarizations induced by adsorption, attractive electrostatic interactions between the dipole of the molecule and the Madelung field of the oxide, etc.

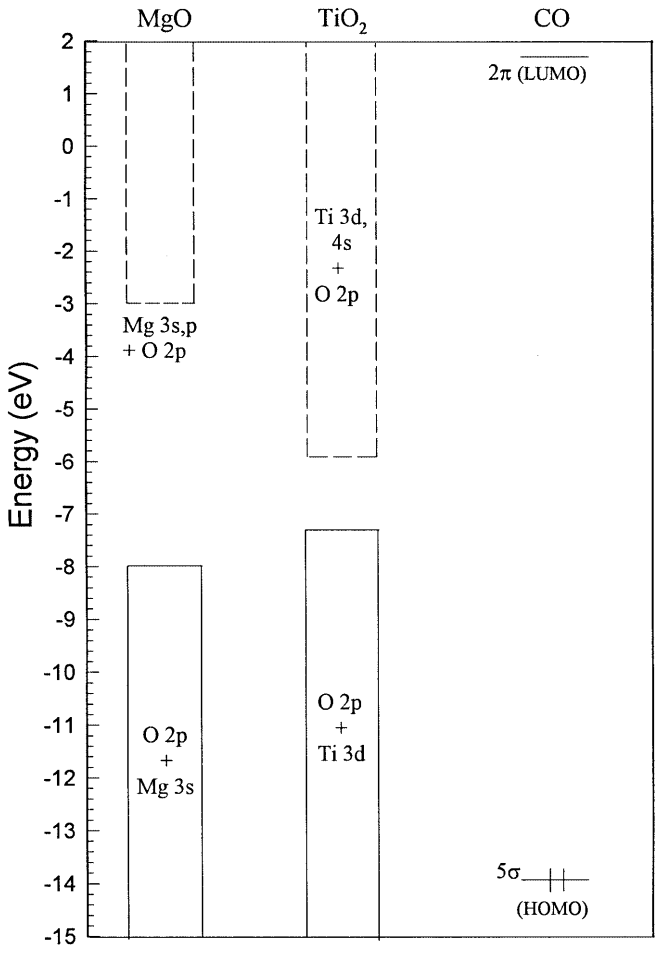

Fig. 2. Energy positions calculated [density functional (*DF*)–generalized gradient approximation (*GGA*)] for the valence and conduction bands of bulk MgO and TiO_2 [31]. The occupied and empty states are denoted by *solid* and *dashed lines*, respectively. For comparison we also include the energies for the frontier orbitals of CO [30]. All the energies are reported with respect to the vacuum level (''0'' of energy)

Thermal desorption mass spectroscopy (TDS) experiments show an adsorption energy of about 3.2 kcal/mol for CO bonded to the cations of MgO(100) [8, 36]. The isosteric heat of adsorption of CO on MgO powder is 3.9 kcal/mol [37]. The results of several theoretical studies for the CO/MgO(100) system are summarized in Table 1. The oxide surface was modeled using finite clusters or slabs, and in many cases DF calculations were performed at the local density approximation or GGA level with different functionals (Becke–Perdew, Becke–Lee–Yang–Parr, Perdew–Wang, Perdew–Burke–Enzerhof). In general, the DF-GGA studies predict CO adsorption energies (2–4 kcal/mol) that are close to the experimental values. The binding energies obtained with the local density approximation (greater than 7 kcal/mol) are too large [23, 43]. The best cluster and slab calculations agree in that there are not noticeable chemical contributions to the bond between CO and the MgO surface [19, 23, 31, 43]. There is a large mismatch in the energy positions of the MgO bands and the CO frontier orbitals (Fig. 2), and the low adsorption energy is mainly due to weak MgO–CO electrostatic interactions (i.e. no significant band-orbital mixing). An analysis of the bonding with the constrained space orbital variation (CSOV) method [19] indicates that, in addition to the effects of electrostatic interactions, CO polarization helps to stabilize the system by reducing Pauli repulsion between the adsorbate and the oxide substrate.

For CO on TiO_2(110), the results of TDS experiments give an adsorption energy of 9.9 kcal/mol [28]. The results of a series of theoretical studies (cluster and slab models) for the CO/TiO_2(110) system are listed in Table 2. The DF calculations at the GGA level give the best agreement with experiment, with the predicted adsorption energies being within 4 kcal/mol of the measured value. On comparing the binding energies in

Table 1. Adsorption of CO on MgO(100). *DF*: density functional; *LDA*: local density approximation; *SCF*: self-consistent field; *GGA*: generalized gradient approximation

Authors	Model	Method	Adsorption energy (kcal/mol)
Nygren et al. [38]	Cluster	Ab initio model potential	1.6–2.1
Pacchioni et al. [39]	Cluster	DF-LDA	11–27
Mejías et al. [19]	Cluster	Ab initio SCF	0.2–3.5
Yudanov et al. [40]	Cluster	DF-GGA	0.5–1.5
Nygren and Pettersson [41]	Cluster	Ab initio model potential	1.8
Chen et al. [42]	Slab	DF-LDA	6.5
Snyder et al. [23]	Slab	DF-LDA	7.4
		DF-GGA	1.9
Rodriguez et al. [30]	Slab	DF-GGA	4.3
		Experimental [36, 37]	3.2–3.9

Table 2. Adsorption of CO on TiO_2(110)

Authors	Model	Method	Adsorption energy (kcal/mol)
Pacchioni et al. [20]	Cluster	Ab initio SCF	18.5–23.5
	Slab	Ab initio SCF	15.7
Casarin et al. [44]	Cluster	DF-GGA	6.7
Sorescu and Yates [28]	Slab	DF-GGA	11.1
Yang et al. [29]	Slab	DF-LDA	18.3
		DF-GGA	5.8
Rodriguez et al. (unpublished)	Slab	DF-GGA	12.2
		Experimental [28]	9.9

Tables 1 and 2 obtained following the same methodology (e.g. see Ref. [30] or Refs. [29, 42]), it is clear that CO adsorbs more strongly on TiO_2(110) than on MgO(100). This can be explained using simple models based on band-orbital mixing [17, 45–47]. One can get an approximate expression for the bonding energy (Q) derived from the interaction between the lowest unoccupied molecular orbital (LUMO) of a closed-shell adsorbate and the occupied states of an oxide

$$Q_{\mathrm{LUMO-OS}} \propto (\beta_{\mathrm{LUMO-OS}})^2/(E_{\mathrm{LUMO}} - E_{\mathrm{OS}}) \ , \qquad (1)$$

where $\beta_{\mathrm{LUMO\text{-}OS}}$ is the resonance integral for the interacting levels, and E_{OS} and E_{LUMO} are the energies of the oxide occupied states and the LUMO, respectively. The corresponding expression for the binding energy that arises from the hybridization of the highest occupied molecular orbital of the adsorbate and the unoccupied sates of the the oxide is

$$Q_{\mathrm{HOMO-US}} \propto (\beta_{\mathrm{HOMO-US}})^2/(E_{\mathrm{US}} - E_{\mathrm{HOMO}}) \ , \qquad (2)$$

where $\beta_{\mathrm{HOMO\text{-}US}}$, $\mathrm{E_{HOMO}}$ and $\mathrm{E_{US}}$ have definitions similar to the terms in Eq. (1). When Eqs. (1) and (2) are applied to the oxides in Fig. 2, the relative positions of the oxide bands indicate that TiO_2 should bond CO more strongly than MgO. The magnitude of the resonance integrals ($\beta_{\mathrm{LUMO\text{-}OS}}$ and $\beta_{\mathrm{HOMO\text{-}US}}$) depends on the overlapping of the orbitals of the adsorbate and the adsorption site and should also favor TiO_2 as a more chemically active oxide [45, 46]. In MgO the cations have a very large positive charge, which leads to orbitals that are more contracted (i.e. smaller β) than the orbitals on cations of an oxide that is not highly ionic like TiO_2. The results of most theoretical calculations show significant band-orbital interactions in the CO/TiO_2(110) system [20, 28–30].

Calculated charge density plots for free CO, the clean TiO_2(110) surface and the CO/TiO_2(110) system are displayed in Fig. 3 [29]. The contour for the clean TiO_2(110) surface exhibits a minimum on top of Ti atoms as a result of a Ti–O electron transfer. The difference in charge density obtained by subtracting the superposition of charge densities in Fig. 3a and b from that in Fig. 3c is plotted in Fig. 3d. Substantial electron accumulation in the region between the carbon and titanium points to the hybridization of the CO(5σ) and Ti($3d$) states [29]. An analysis of the bonding with the CSOV method [20] shows that CO binds to Ti centers of TiO_2 through essentially two mechanisms: CO polarization in response to the surface electric field and CO σ donation to the adsorption site. The initial electrostatic attraction between the adsorbate and oxide is almost exactly offset by Pauli repulsion [20].

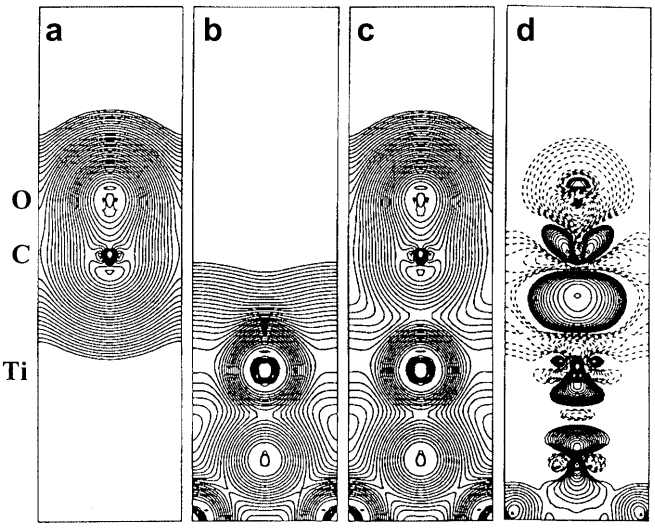

Fig. 3. The calculated valence charge densities for **a** the CO monolayer, **b** the TiO_2(110) clean surface, **c** the CO/TiO_2(110) system and **d** the charge-density difference obtained by subtracting the superposition of the charge densities of the CO monolayer and TiO_2(110) from that of CO/TiO_2(110). The dashed lines **d** indicate negative differences (taken from Ref. [29])

Results of TDS give adsorption energies of 5.1 and 8.4 kcal/mol for NO on MgO(100) [8, 36] and TiO_2(110) [48], respectively. DF slab calculations at the GGA level (Perdew–Wang 91 functional) predict NO adsorption energies of 5.9 kcal/mol on MgO(100) [30] and 10.5 and 11.6 kcal/mol on TiO_2(110) [48, 49]. As in the case of CO adsorption, TiO_2 bonds NO more strongly than MgO. For NO on MgO(100), the bonding involves weak adsorbate–surface electrostatic interactions and there is no substantial mixing of the frontier orbitals of the molecule with the bands of the oxide [30]. In contrast, there is band-orbital mixing in the NO/TiO_2(110) system [48] that leads to a larger binding energy.

The role of surface defects and imperfections on the behavior of CO and NO on oxides has been the subject of several theoretical studies [30, 43, 48, 49, 50, 51]. For compounds such as TiO_2 and CeO_2, the creation of O vacancies is not difficult and induces occupied metal states above the valence band of the oxide [1, 52]. This interesting phenomenon is illustrated in Fig. 4. After removing O atoms from the first layer of a TiO_2(110)

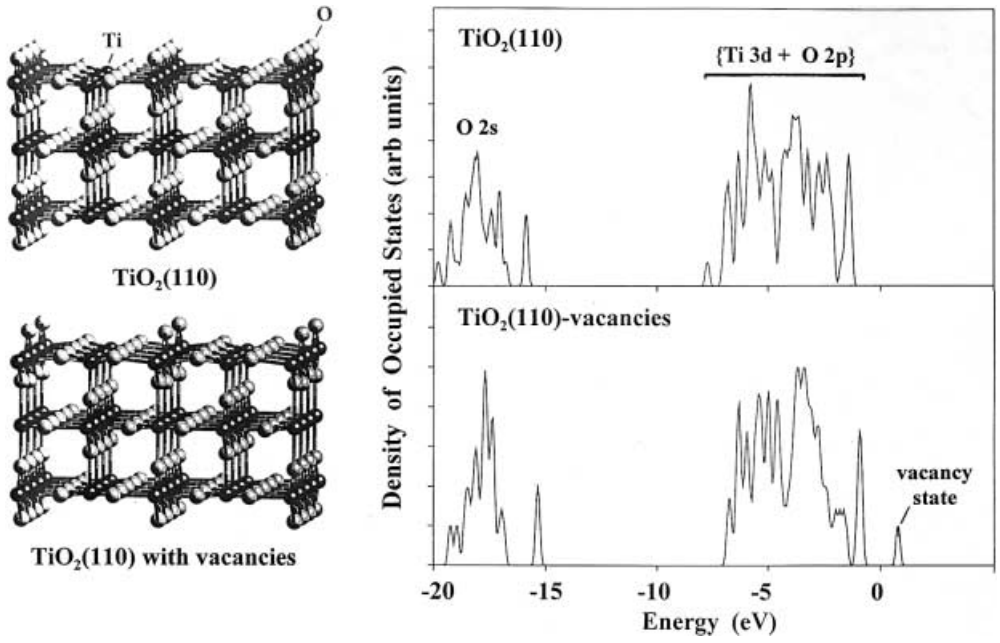

Fig. 4. *Left*: Three-layer slab models for TiO_2(110) and a TiO_{2-x}(110) surface with O vacancies. *Right*: Calculated density of states for the occupied bands of the TiO_2(110) and TiO_{2-x}(110) slabs (taken from Ref. [35]). The "0" of energy is not the vacuum level [25]

slab, an extra state appears about 2 eV above the top of the {O $2p$ + Ti $3d$} band and has Ti $3d$ character [35]. This state has been observed in experiments of valence photoemission [1, 35, 49]. According to Eq. (1), the system with O vacancies should be more chemically active than the stoichiometric system. Indeed, experimental and theoretical studies indicate that TiO_{2-x}(110) interacts more strongly with CO or NO than a perfect TiO_2(110) surface [44, 48, 49].

3 Adsorption of sulfur-containing molecules on oxides

A fundamental understanding of the interaction of sulfur-containing molecules with oxide surfaces is important for two reasons. First, oxides are used as sorbents or catalysts to remove sulfur-containing molecules from oil and to prevent the evolution into the atmosphere of the SO_2 formed as a by-product during the combustion of fuels [53, 54]. Second, in several operations in the semiconductor industry, sulfur is deposited on oxide surfaces to passivate or protect electronic devices [7]. Thus, for practical reasons it is very important to establish which types of oxides have high reactivity towards sulfur-containing molecules. The sulfur uptake (HS + S) for the dissociative adsorption of hydrogen sulfide on metal centers of a series of oxides at 300 K [31, 53, 55] is shown in Fig. 5. The band gap for each oxide is reported in parentheses. There is a clear qualitative correlation: the smaller the band gap in an oxide, the bigger its reactivity towards H_2S. Identical behavior was observed for the adsorption of S_2 [55, 56].

In general, the strength of the bond between H_2S and an oxide depends on the interactions between the dipole of the molecule and the electrostatic field generated by the charges in the oxide, plus the mixing of the frontier orbitals of the molecule with the conduction and valence bands of the oxide [1, 55]. Photoemission experiments

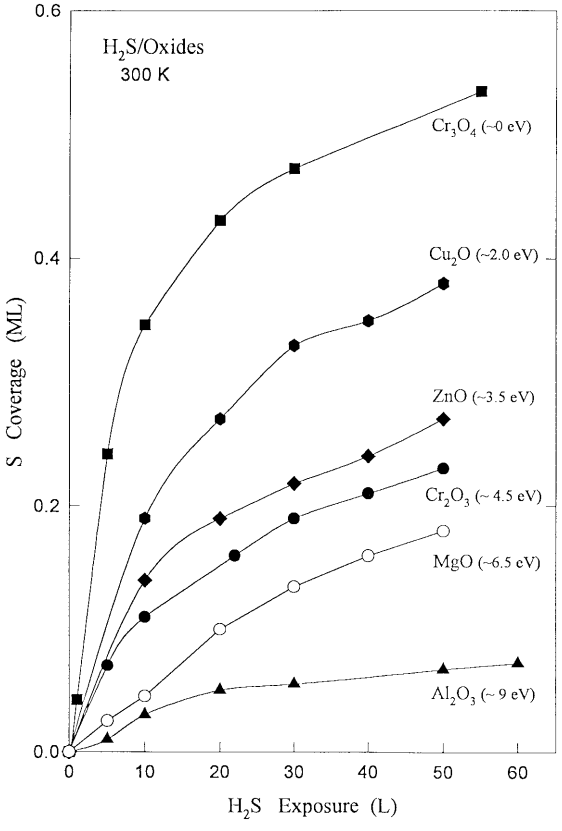

Fig. 5. Total sulfur uptake (HS + S) for the dissociative adsorption of hydrogen sulfide (H_2S) on metal centers of a series of oxides at 300 K [31, 53, 55]. The band gap for each oxide is reported in *parentheses*

indicate that H_2S preferentially reacts with the metal centers of the oxides in Fig. 5 [31, 53, 55]. Thus, electrostatic interactions should take place between the negative sulfur ($S^{\delta-}$) in the molecule and the positive

metal ions ($M^{\Delta+}$) in the oxides. The electrostatic interactions are expected to be particularly strong on oxides that have a large degree of ionicity, such as Al_2O_3 and MgO [33, 43]. Interestingly, these oxides exhibit the lowest reactivities in Fig. 5. On the other hand, oxides that are not highly ionic, such as ZnO or Cu_2O, display substantial reactivity. Thus, it is very difficult to explain the trends in Fig. 5 in terms of electrostatic bonding between H_2S and the oxides. Clearly, the chemical activity of an oxide probably depends on how well its bands mix with the orbitals of H_2S, and the electrostatic interactions with the dipole moment of H_2S play only a secondary role.

The energy positions for the valence and conduction bands of bulk Al_2O_3, MgO, ZnO and Cu_2O are shown in Fig. 6. To generate this figure, we used values reported in the literature for the electronic properties of the oxides [1, 22] instead of theoretical results. DF calculations predict the same trends but underestimate the magnitude of the band gaps by 1–2 eV [22, 31]. This is a common problem with DF calculations [57]. For the oxides in Figs. 2 and 6, when the band gap increases the valence band moves towards higher binding energy, while at the same time there is a decrease in the stability of the conduction band. Simple models based on band-orbital mixing [22, 31, 45–47], i.e. Eqs. (1) and (2), would predict that the smaller the band gap in an oxide, the larger its chemical reactivity. In general terms, this agrees with the behavior seen in Fig. 5 and with results obtained in a series of theoretical works [22, 31, 55, 56]. The qualitative correlation seen between the band-gap size and reactivity of an oxide also involves the ionicity of the system. For the oxides in Fig. 6, the degree of ionicity and the size of the band gap go together, and the highly ionic systems offer metal centers whose orbitals are relatively small and have energies that do not match well with those of the orbitals of an adsorbate [22, 55].

DF slab calculations have been used to study in detail the reaction of H_2S with MgO(100) and ZnO(0001) surfaces [22]. MgO and ZnO are frequently employed in industry for trapping sulfur-containing impurities present in chemical feedstocks and the SO_2 formed after burning oil- or coal-derived fuels [5, 58]. Plots of the electron density around surface atoms of MgO(100) and ZnO(0001) are shown in Figs. 7 and 8. In the case of MgO(100), the total electron density on the magnesium atoms is small and the electron density plot is dominated by maxima located on top of the oxygen atoms. Such is not the case for

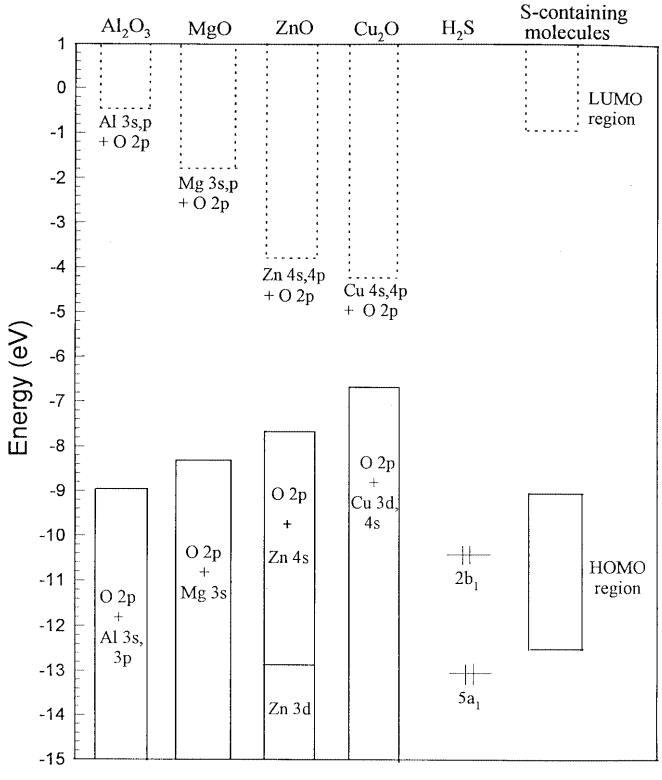

Fig. 6. Energy positions for the valence and conduction bands of bulk Al_2O_3, MgO, ZnO and Cu_2O (taken from Ref. [22]). The empty and occupied states are indicated by *dotted* and *solid lines*, respectively. For comparison we also include the energies for molecular orbitals of H_2S, $5a_1$ and $2b_1$ (HOMO), and other sulfur-containing molecules (thiols and thiophenes). Not shown in the figure is the LUMO of H_2S, $3b_2$ orbital, which is located at about 4 eV. All the energies are reported with respect to the vacuum level ("0" of energy)

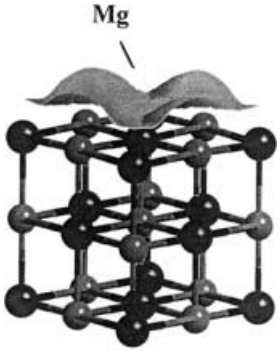

Fig. 7. Calculated (DF-GGA) electron-density plot for a MgO(100) surface. For simplicity, only a few metal and oxygen atoms of the system are shown (taken from Ref. [22])

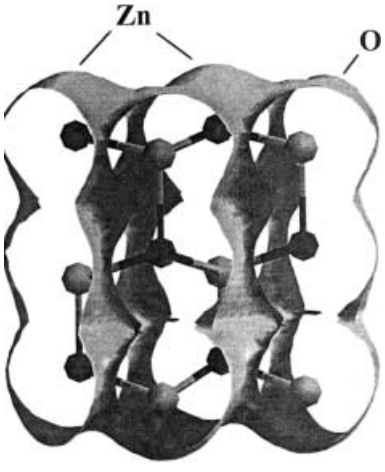

Fig. 8. Calculated (DF-GGA) electron-density plot for a ZnO(0001) surface. For simplicity, only a few Zn and O atoms of the system are shown (taken from Ref. [22])

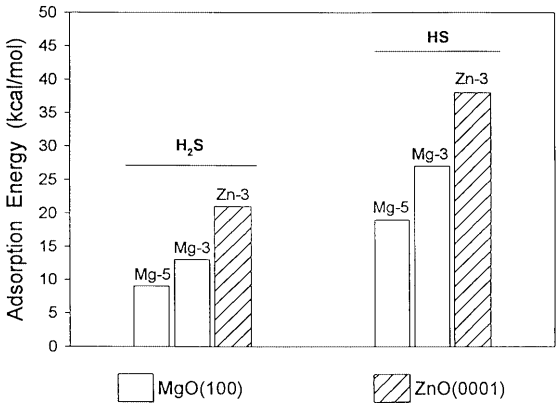

Fig. 9. Calculated adsorption energies (DF-GGA [22]) for H_2S and HS on MgO(100) (*white bars*) and ZnO(0001) (*hatched bars*). In the case of MgO, results are shown for adsorption on penta- and tricoordinated metal centers (Mg-5 and Mg-3, respectively)

ZnO(0001), where one can see a large electron density around the zinc atoms. Thus, from an electronic viewpoint, ZnO(0001) is better suited to respond to the presence of sulfur-containing molecules than MgO(100).

Calculated adsorption energies [22] for H_2S and HS on MgO(100) and ZnO(0001) are shown in Fig. 9. In the case of MgO, results are shown for adsorption on pentacoordinated (Mg-5) sites of a flat terrace and on tricoordinated (Mg-3) sites of a step. The DF results [22] indicate that atomic S and HS form strong bonds on a perfect MgO(100) surface (adsorption energies of 34 and 19 kcal/mol, respectively), but the bonding interactions of the H_2S molecule are relatively weak (9 kcal/mol). For the dissociative chemisorption of H_2S on two adjacent Mg and O sites of the flat oxide surface,

$$H_2S_{gas} + Mg_{surface} + O_{surface} \rightarrow HS\text{-}Mg_{surface} + H\text{-}O_{surface} \ , \quad (3)$$

a ΔE of –14 kcal/mol (exothermic reaction) is predicted [22]. Thus, dissociation of the molecule is an energetically favorable process, but it may not be easy owing to the lack of strong interactions between H_2S and the flat oxide surface. The Mg-3 atoms in steps of MgO(100) have a larger electron density [22] and occupied states at higher energy [59] than Mg-5 atoms in a terrace. On the Mg-3 sites, the adsorption energy of H_2S increases to 13 kcal/mol. This energy is still smaller than the value of 21 kcal/mol found for H_2S on ZnO(0001) [22]. After comparing the adsorption energies in Fig. 10, it is clear that ZnO(0001) should be a better sorbent for H_2S than MgO(100). Indeed, the experimental results in Fig. 5 show that at 300 K the rate of dissociation of H_2S on ZnO is larger than on MgO.

The band gaps of ZnO and TiO_2 are similar (3.4 and 3.1 eV, respectively [1]) and both oxides are ionocovalent [20, 22, 34, 35]. In agreement with the predictions of Eqs. (1) and (2), DF calculations give comparable adsorption energies for S atoms on ZnO(0001) [22] and TiO_2(110) [35]: 59 and 64 kcal/mol, respectively. The creation of O vacancies in TiO_2(110) produces occupied states above the valence {O $2p$ + Ti $3d$} band, effectively reducing the band gap of the oxide (Fig. 4) and making it more reactive. The calculated adsorption energy for S on these defect sites is 18 kcal/mol higher than for adsorption on a perfect TiO_2(110) surface. This is consistent with experimental results of high-resolution photoemission and thermal desorption [35], which show preferential bonding of S to Ti centers near O vacancies in TiO_{2-x}(110).

4 Adsorption of alkali metals on oxides

Alkali/oxide interfaces play an important role in catalysis, materials science, electrochemistry, geochemistry, the fabrication of sensors and solar cells, etc. [1, 3, 11, 13, 60]. Experimental studies indicate that the electronic interactions between an alkali metal and an oxide can range from very strong to weak [11, 13, 61]. In principle, alkalis can interact with oxygen or metal centers of an oxide but, since they are very electropositive elements [62], usually the alkali–oxygen interactions are stronger [63, 64]. The bonding of alkalis to MgO(100) [65, 66], ZnO(0001) [63, 64], ZnO(000$\bar{1}$) [63, 64] and TiO_2(110) [67, 68, 69] has been examined using different theoretical approaches.

In general, band-orbital interactions determine the strength of the adsorption bond for the alkali. On MgO(100), there is a large band gap and the electron-acceptor states in the conduction band are not stable enough (Figs. 2, 6) to receive electron density from the alkali. This leads to nonionic and relatively weak adsorption bonds [65, 66], and in many cases the alkali prefers to form three-dimensional particles instead of bonding to the oxide substrate [11, 70]. For ZnO(000$\bar{1}$) and TiO_2(110), the electron-acceptor states in the conduction bands are more stable than in MgO(100) (Figs. 2, 6). On ZnO(000$\bar{1}$) and TiO_2(110), there is a large alkali–surface charge transfer and strong adsorption bonds [63, 64, 67–69]. In the case of K/TiO_2(110) [67, 69], cluster and slab calculations (ab initio HF, DF-GGA methods) show a charge transfer from the K $4s$ level to the empty $3d$ levels of fivefold coordinated surface Ti atoms. The potential-energy surface for the motion of the adsorbed potassium ions is rather flat, and the structure of the overlayer is largely determined by adsorbate–adsorbate repulsive interactions [67, 69]. Potassium prefers to adsorb in the vicinity of the protruding bridging oxygens at very low coverages [67]. At high coverages, the results of molecular dynamics simulations show rather complex structures where K^+ ions preferentially sit on the threefold hollow sites formed by two bridging and one planar oxygen [69].

The adsorption of an alkali on an oxide usually leads to the appearance of occupied electronic states within the band gap of the oxide [66, 67, 69]. For example, in K/TiO_2(110), the alkali–oxide charge transfer produces occupation of the Ti $3d$ levels and a new state appears about 2 eV above the {Ti $3d$ + O $2p$} valence band [67, 69, 71, 72]. For the Na/MgO system, there is no alkali–oxide charge transfer [65, 66], but occupied states of the alkali are located in the band gap of MgO (Fig. 10) [66]. These phenomena considerably increase the reactivity of oxide surfaces [64, 66, 73–75]. The electronic states

induced by alkali adsorption are energetically better positioned for bonding interactions with the orbitals of reactant molecules than the occupied bands of pure oxides (Fig. 10) [64, 66, 75]. For this reason, alkali adatoms enhance the reactivity of ZnO surfaces towards sulfur-containing molecules (H_2S [73], S_2 [73], thiophene [75], SO_2 [64]). MgO is not active for the dissociation of SO_2 in DeSOx operations [54, 76–78], but the addition of Na to the oxide surface makes possible interactions with the LUMO of the reactant molecule (S–O antibonding, Fig. 10) facilitating the breaking of S–O bonds [66].

5 Engineering of mixed-metal oxides

Mixed-metal oxides are frequently used in many areas of chemistry, physics and materials science [1, 3, 79, 80]. In principle, the combination of two metals in an oxide matrix can produce materials with novel chemical and physical properties that can lead to a superior performance in technological applications. The two metals can behave as "isolated units" that bring their intrinsic properties to the system, or their behavior can be modified owing to the effects of metal–metal or metal–oxygen–metal interactions [30, 81, 82]. In this respect, it is important to understand how to choose the "right" combination of metals. Recent theoretical studies have addressed this issue [30, 81–88]. The main objective is to obtain a fundamental knowledge useful for engineering mixed-metal oxides [30, 81, 82]. The results and discussion presented earlier suggest that the surface reactivity of a mixed-metal oxide could be determined by the hybridization of the oxide bands and adsorbate orbitals. In this section, we explore the validity of this hypothesis and show that this simple concept is useful for predicting the chemical behavior of mixed-metal oxides.

Molybdenum is able to form stable oxides in combination with many metals ($MeMoO_4$ compounds; Me = Mg, Pb, Mn, Fe, Co, Ni, Zn) [79, 89, 90]. These molybdates are ideal for studying the behavior of mixed-metal oxides and constitute an interesting group on their own because of their structural, electronic and catalytic properties [79, 89, 90, 91, 92, 93]. The left-hand panel in Fig. 11 shows calculated (DF-GGA) density-of-states plots for β-$MgMoO_4$, β-$NiMoO_4$, and β-$FeMoO_4$. Only occupied states are included in the graph. β-$NiMoO_4$ displays a large density of states near the top of the valence band that is not observed for β-$MgMoO_4$. In this respect, β-$FeMoO_4$ is an intermediate case between β-$NiMoO_4$ and β-$MgMoO_4$. Also, the Ni 3d states in β-$NiMoO_4$ are energetically less stable than the Fe 3d states in β-$FeMoO_4$ or the Mg 3s states in β-$MgMoO_4$. These trends suggest that $NiMoO_4$ should be more chemically active than $FeMoO_4$ or $MgMoO_4$ [81, 83]. The right-hand panel in Fig. 11 displays results of X-ray absorption near-edge spectroscopy (XANES) collected after dosing the same amount of H_2S to β-$NiMoO_4$, β-$FeMoO_4$, and β-$MgMoO_4$ at 400 °C [83]. The molybdates were only partially sulfided, and the XANES data indicate that their chemical reactivity increases in the sequence: $MgMoO_4 < FeMoO_4 < NiMoO_4$ [83]. An identical sequence is obtained after analyzing experimental results for the reaction of H_2 with the molybdates [83, 93, 94]. Thus, a clear correlation is seen between the electronic and chemical properties of these compounds, which can be explained in terms of variations in the magnitude of band-orbital mixing [81, 83, 95].

At low concentrations, many transition metals form solid solutions in magnesium oxide ($TM_xMg_{1-x}O$, TM = Cr, Mn, Fe, Co, Ni, Rh, Pd, Pt, etc.) [96, 97]. In these solid solutions, the second metal (dopant agent) occupies magnesium sites within the typical rock salt structure of MgO. Metal-doped MgO is active as a catalyst for the oxidative coupling of methane to pro-

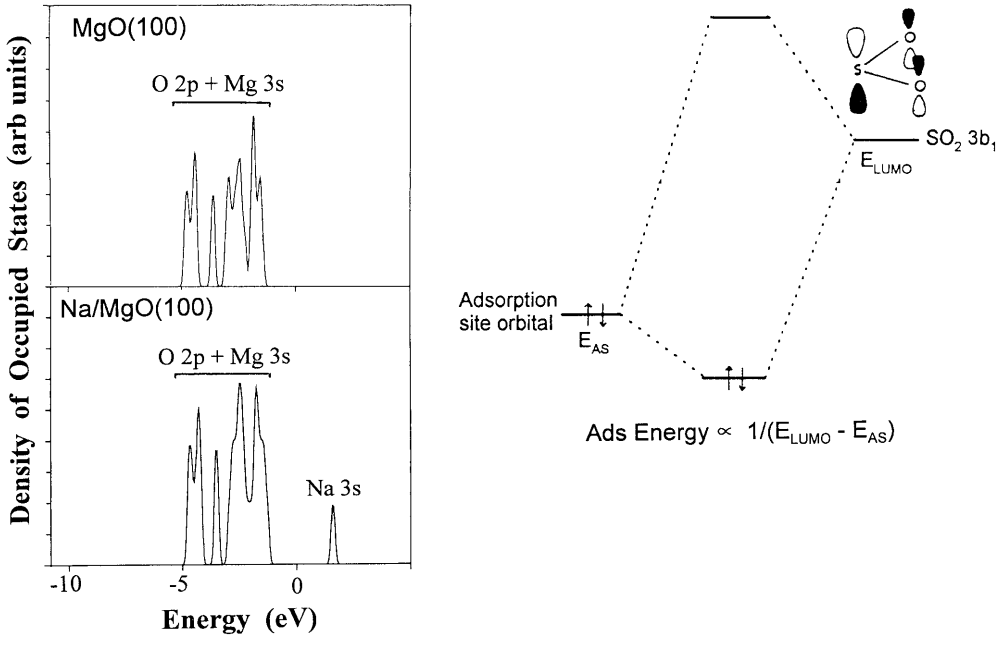

Fig. 10. *Left*: Calculated (DF-GGA) density of states for the occupied bands of MgO(100) and Na/MgO(100). The "0" of energy is not the vacuum level [25]. *Right*: Orbital interactions for the bonding of SO_2 to a surface metal center. The smaller the energy separation between the interacting levels (E_{LUMO}–E_{ads}), the bigger the adsorption energy of SO_2 (taken from Ref. [66])

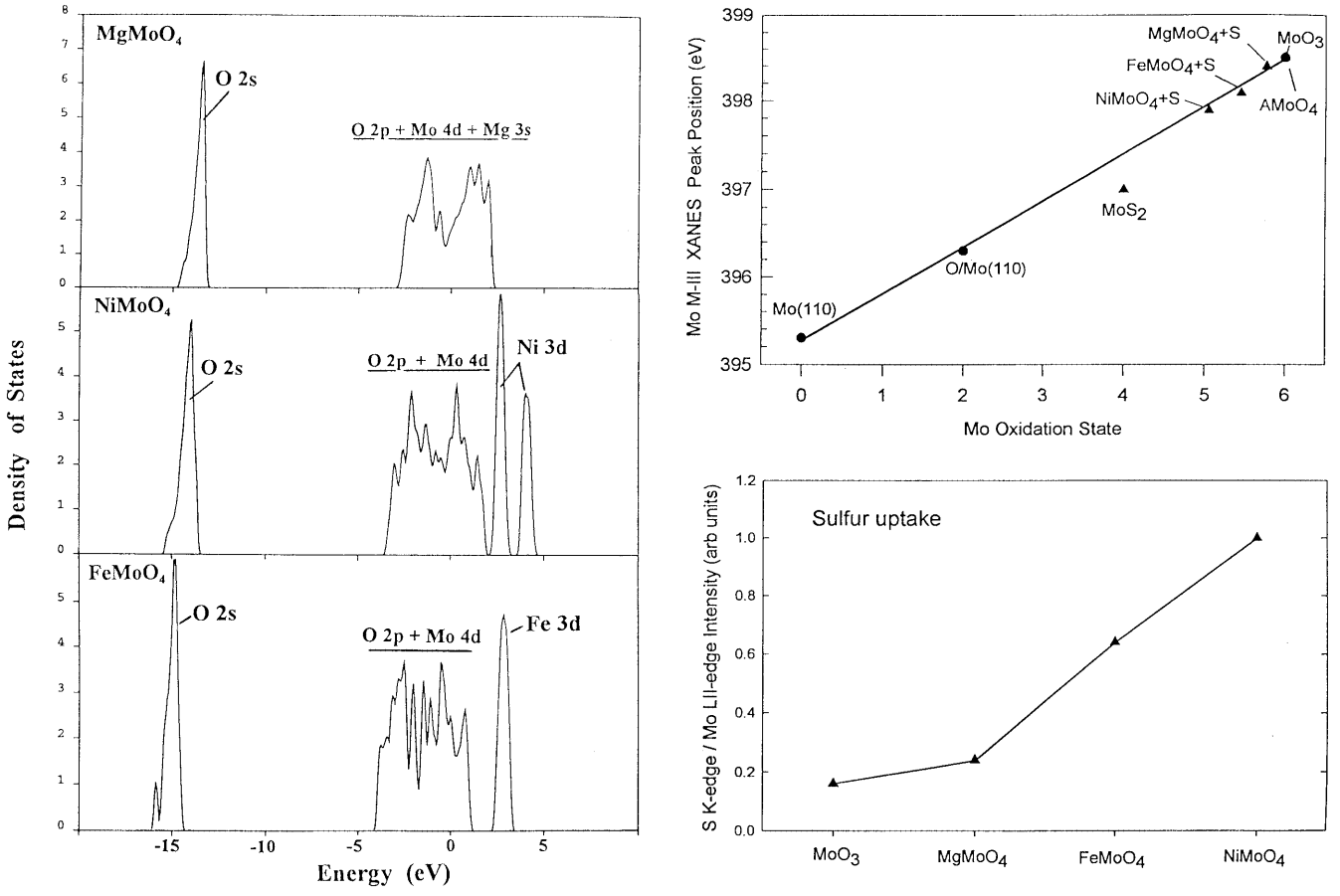

Fig. 11. *Left*: Calculated (DF-GGA) density of states for the occupied bands of β-$MgMoO_4$, β-$NiMoO_4$ and β-$FeMoO_4$. The "0" of energy is not the vacuum level [25]. *Right*: Results of X-ray absorption near-edge spectroscopy for the adsorption of H_2S on MoO_3, β-$MgMoO_4$, β-$NiMoO_4$ and β-$FeMoO_4$ at 400 °C (taken from Ref. [83])

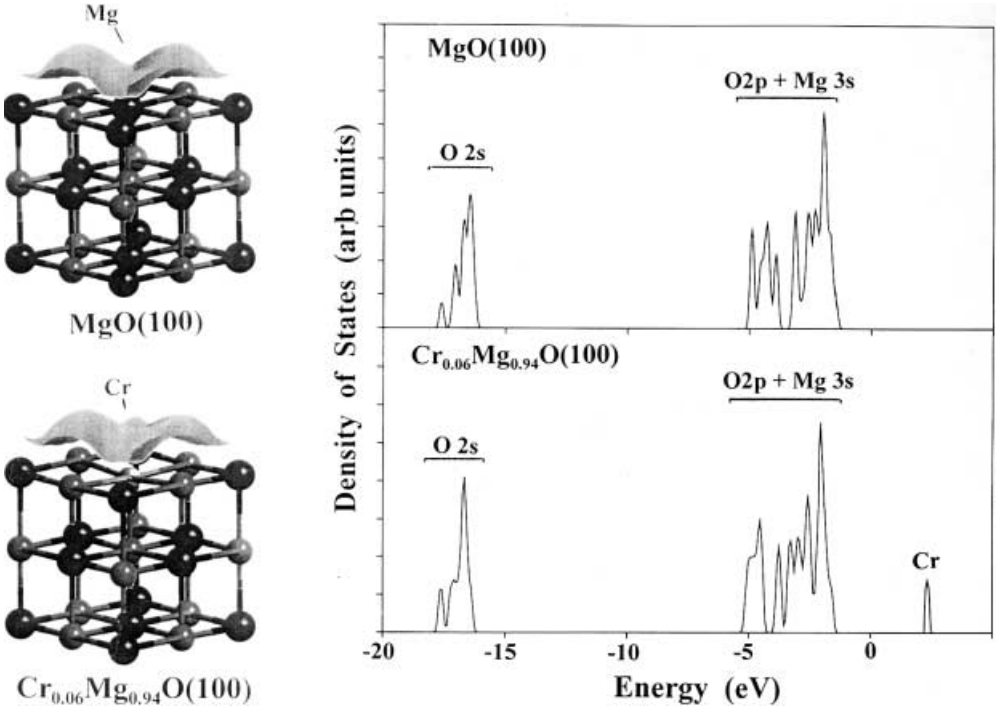

Fig. 12. *Left*: Calculated (DF-GGA) electron-density plots for MgO(100) (*top*) and $Cr_{0.06}Mg_{0.94}O(100)$ (*bottom*) surfaces. For simplicity, only a few metal and oxygen atoms of the surfaces are shown. *Right*: Calculated density of states for the occupied bands of the MgO(100) and $Cr_{0.06}Mg_{0.94}$ O(100) systems. The "0" of energy is not the vacuum level (taken from Ref. [102])

duce C_2 hydrocarbons [98, 99], the reforming of CH_4 with CO_2 or H_2O [96, 100], DeNOx [3, 101] and DeSOx processes [102]. Big variations in catalytic activity have been observed when changing the second metal or dopant agent [98, 100–104]. Thus, from a practical viewpoint, it is quite important to know what determines the chemical reactivity of metal-doped MgO. This problem has been studied using DF slab calculations [30, 101–103].

The $Cr_xMg_{1-x}O$ ($x = 0.03$–0.06) system is particularly interesting because it illustrates how an element in a mixed-metal oxide can have an enhanced chemical activity [30, 102]. $Cr_xMg_{1-x}O$ is a better catalyst than MgO or Cr_2O_3 for the Claus process ($2H_2S + SO_2 \rightarrow 2H_2O + 3S_{solid}$) and the reduction of SO_2 by CO ($SO_2 + 2CO \rightarrow 2CO_2 + S_{solid}$) [102]. DF calculations indicate that this is a consequence of the special electronic properties for Cr cations contained in a matrix of MgO [102]. These Cr atoms have a lower oxidation state than the atoms in Cr_2O_3. Plots of the electron density around Mg and Cr surface atoms in MgO(100) and $Cr_{0.06}Mg_{0.94}O$ (100) are shown in Fig. 12 [102]. For MgO(100), the electron density on the Mg centers is small [19, 22, 32, 33] and dominant maxima are located on top of the oxygens. In contrast, for $Cr_{0.06}Mg_{0.94}O$ (100), one finds a substantial electron density around the Cr atoms. Figure 12 also displays calculated density-of-states plots for the occupied bands in MgO(100) and $Cr_{0.06}Mg_{0.94}O$ (100). In the mixed-metal oxide, the occupied Cr 3*d* levels are less stable energetically than the levels in the occupied {O $2p$ + Mg $3s$} bands of MgO; thus, from an electronic viewpoint, the Cr centers in a $Cr_{0.06}Mg_{0.94}O$ (100) surface are very well suited to respond to the presence of adsorbates.

Equation (1) indicates that an important parameter to consider when designing a mixed-metal oxide and trying to control its chemical reactivity is the final energy position of the occupied states in the oxide system. The top panel in Fig. 13 shows the relative position of the dopant levels in a series of $TM_{0.06}Mg_{0.94}O$ (100) surfaces (TM = Cr, Mn, Fe, Co, Ni, Zn, Sn) [101]. In these mixed-metal oxides, the instability of the TM 3*d* band increases as one moves from right to left in the 3*d* series. The effects of an early transition metal on the electronic properties of MgO are stronger than those of *s*,*p* metals such as Zn or Sn. The predicted trends agree well with experimental results of valence photoemission for $Zn_{0.06}Mg_{0.94}O$, $Ni_{0.06}Mg_{0.94}O$, $Fe_{0.06}Mg_{0.94}O$ and $Cr_{0.07}Mg_{0.93}O$ [30, 101, 103]. The bottom panel in Fig. 13 shows the values calculated (DF-GGA) for the adsorption energy of NO on the $TM_{0.06}Mg_{0.94}O$(100) mixed-metal oxides. Clearly, there is a relationship between the energy position of the dopant electronic levels and the chemical reactivity of a mixed-metal oxide. This relationship is not linear, because one must also consider the number of states with low stability provided by a dopant agent [30, 101]. In addition, several factors can affect the strength of a metal-NO bond [46, 104–106].

The type of correlation seen in Fig. 13 and in thermal desorption measurements for NO adsorption [30, 103] has also been observed for other adsorbates interacting with mixed-metal oxides [30, 101, 102, 103]. DF results for the

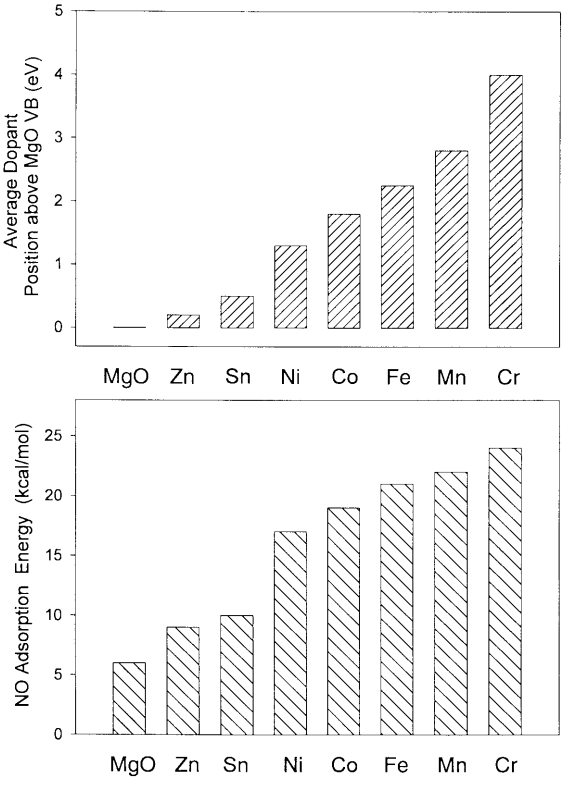

Fig. 13. *Top*: DF-calculated average position for the dopant levels in $TM_{0.06}Mg_{0.94}O$(100) surfaces (TM = Zn, Sn, Ni, Co, Fe, Mn, Cr). The values reported are with respect to the top of the valence band (see Fig. 12). *Bottom*: Calculated (DF-GGA) adsorption energy for NO on $TM_{0.06}Mg_{0.94}O$(100) surfaces (taken from Ref. [101])

adsorption of CO [30], NO [30, 101], H_2S [22, 102] and SO_2 [77, 102] on $Ni_{0.06}Mg_{0.94}O$(100) and $Cr_{0.06}Mg_{0.94}O$(100) surfaces are compared in Fig. 14. In general, tri- or tetracoordinated magnesium atoms (Mg-3 and Mg-4 in our notation) in step sites of MgO(100) are more reactive than pentacoordinated magnesium atoms (Mg-5) located in large terraces of the oxide surface. After doping MgO with Ni and Cr, there is an increase in chemical activity, with the effects of Cr being larger. As for the results in Figs. 11 and 13, a good correlation is observed between the chemical and electronic properties of the mixed-metal oxides: the less stable the occupied levels of an oxide, the higher its chemical reactivity. This correlation is probably valid in general, since we are dealing with adsorbates that bond in different ways. Thus, an important parameter to consider when engineering a mixed-metal oxide is the final energy position of the occupied states provided by the second metal or dopant agent. In this aspect, theoretical methods can be very useful for making predictions and avoiding mistakes usually associated with the empirical design of mixed-metal oxides [30, 101–103].

A dopant agent can enhance the chemical activity of a host oxide by facilitating the formation of O vacancies [52, 82]. For example, doping of ceria (CeO_2) with Zr, Ti or Ca induces a relatively minor narrowing of the band gap (less than 1 eV), and no occupied states appear well above the host valence band (Fig. 15) [52]. However, the dopants

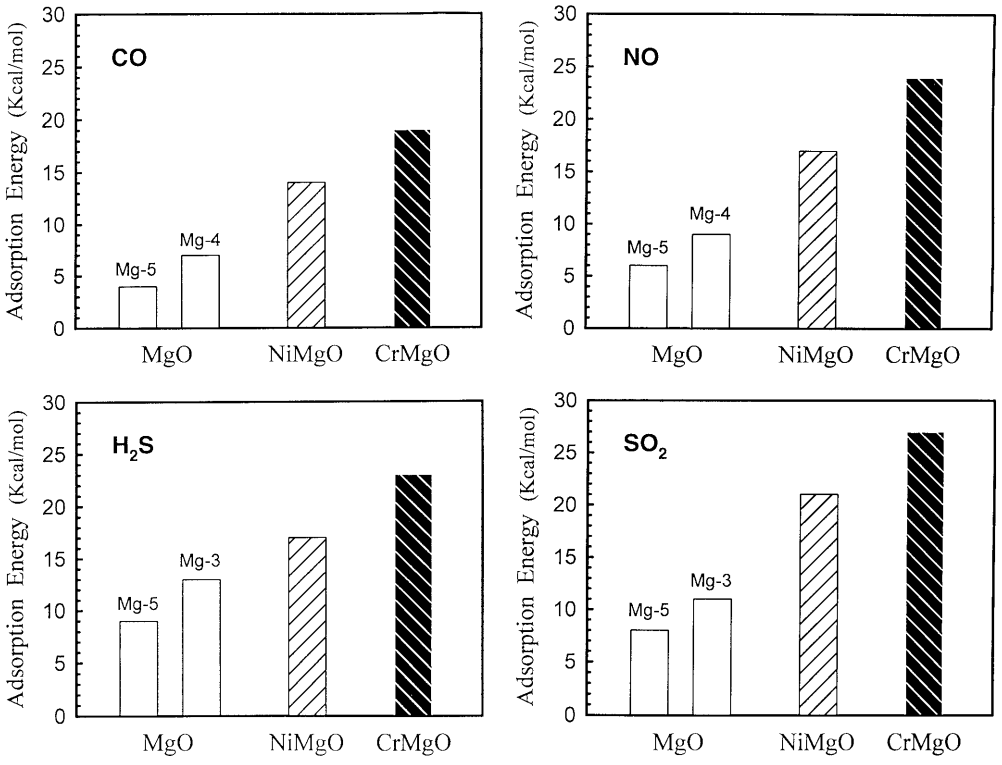

Fig. 14. DF results for the adsorption of CO, NO, H_2S and SO_2 on metal centers of MgO(100), $Ni_{0.06}Mg_{0.94}O(100)$ and $Cr_{0.06}Mg_{0.94}O(100)$ surfaces. In the case of MgO, results are shown for the adsorption of the molecules on pentacoordinated magnesium atoms (Mg-5) of (100) terraces and tri- or tetracoordinated magnesium atoms (Mg-3 or Mg-4) at step sites of the MgO(100) surface. The values reported for the mixed-metal oxides are for pentaco-ordinated Ni or Cr atoms (taken from Ref. [30])

produce structural perturbations in the lattice of ceria that make easier a loss of oxygen [52, 82, 107], which leads to the appearance of Ce 4*f* occupied states about 2 eV above the CeO_2 valence band (Fig. 15). These "Ce^{3+}" states are well positioned for bonding interactions with orbitals of adsorbates [51, 52, 82]. Several metal oxides are expected to be useful candidates as host matrixes for oxygen vacancy engineering through metal doping, for example, oxides of Bi, Mo, Nb, Ti, V, W and Zr [82].

6 Conclusions

Recent advances in theoretical methods (mainly based on DF theory) have made it possible to study in a quantitative or semiquantitative way a series of phenomena associated with the bonding of molecules to oxides [9, 19, 20, 22, 29]: band-orbital hybridizations and subsequent electron transfer between adsorbate and surface, effects of Pauli repulsion, charge polarizations induced by adsorption, attractive electrostatic interactions between the dipole of the molecule and the Madelung field of the oxide, etc. In many cases, this has led to a fundamental understanding of the chemistry of oxide surfaces. However, many problems in this area remain a challenge [14, 15, 43, 108, 109], and the approximate nature of most theoretical methods makes necessary a close coupling of theory with experiment. Following this multidisciplinary approach, the importance of band-orbital interactions for the reactivity of oxide surfaces has become clear. Simple models based on band-orbital mixing [17, 45–47] can explain trends found for the adsorption of CO, NO, alkali atoms, and sulfur-containing molecules on oxide surfaces. These simple

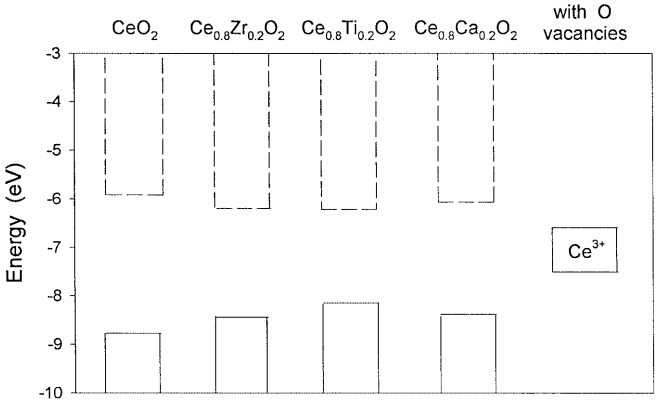

Fig. 15. Energy positions for the valence and conduction bands of CeO_2, $Ce_{0.8}Zr_{0.2}O_2$, $Ce_{0.8}Ti_{0.2}O_2$ and $Ce_{0.8}Ca_{0.2}O_2$ (DF-GGA). The empty and occupied states are indicated by *dashed* and *solid lines*, respectively. The *right side* of the figure shows the position for the occupied "Ce^{3+}" states when O vacancies are introduced in the oxides (taken from Ref. [52])

models provide a conceptual framework for modifying or controlling the chemical activity of pure oxides, and for engineering mixed-metal oxides. In this respect, theoretical calculations can be very useful for predicting the best ways for enhancing the reactivity of oxide systems and reducing the waste of time, energy and materials characteristic of an empirical design [30, 82, 101–103].

Acknowledgements. In the past few years a great number of people have been helpful in discussing the problems associated with the behavior of molecules on oxide surfaces. Special thanks to J. Hrbek and A. Maiti for many thought-provoking conversations. I am also

grateful to J. Brito, S. Chaturvedi, J. Dvorak, J. Evans, L. González, J. Hanson, M. Kuhn, T. Jirsak, J.Z. Larese, H. Lee and M. Pérez for helpful discussions. This work was carried out at Brookhaven National Laboratory under contract DE-AC02-98CH10086.

References

1. Henrich VA, Cox PA (1994) The surface science of metal oxides. University Press, Cambridge
2. Wyckoff RWG (1964) Crystal structures, 2nd edn. Wiley, New York
3. Kung HH (1989) Transition metal oxides: surface chemistry and catalysis. Elsevier, Amsterdam
4. Ertl G, Knözinger H, Weitkamp J (eds) (1997) Handbook of heterogeneous catalysis. Wiley-VCH, Weinheim
5. Slack AV, Hollinden GA (1975) Sulfur dioxide removal from waste gases, 2nd edn. Noyes Data Corporation, New Park, NJ
6. Shelef M, Graham GW (1994) Catal Rev Sci Eng 36: 433
7. Sherman A (1987) Chemical vapor deposition for microelectronics: principles, technology and applications. Noyes, Park Ridge, NJ
8. Freund HJ (1999) Faraday Discuss 114: 1
9. Rodriguez JA, Chaturvedi S, Kuhn M, Hrbek J (1998) J Phys Chem B 102: 5511
10. Street SC, Xu C, Goodman DW (1997) Annu Rev Phys Chem 48:43
11. Campbell CT (1997) Surf Sci Rep 27: 1
12. Barteau MA (1996) Chem Rev 96: 1413
13. Madey TE, Akshinsky BV, Ageev VN, Johnson RE (1998) J Geophys Res 103: 5873
14. Madey TE (1999) Faraday Discussi 114: 461
15. Freund HJ, Kuhlenbeck H, Staemmler V (1996) Rep Prog Phys 59: 283
16. Whitten JL, Yang H (1996) Surf Sci Rep 24: 55
17. van Santen RA, Neurock M (1995) Catal Rev Sci Eng 37: 557
18. Hammer B, Nørskov JK (2000) Adv Catal 45: 71
19. Mejías JA, Márquez AM, Fernández-Sanz J, Fernández-Garcia M, Ricart JM, Sousa C, Illas F (1995) Surf Sci 327: 59
20. Pacchioni G, Ferrari AM, Bagus PS (1996) Surf Sci 350: 159
21. Anchell JL, Hess AC (1996) J Phys Chem 100: 18317
22. Rodriguez JA, Maiti A (2000) J Phys Chem B 104: 3630
23. Snyder JA, Alfonso DR, Jaffe JE, Lin Z, Hess AC, Gutowski M (2000) J Phys Chem B 104: 4717
24. Rodriguez JA, Ricart JM, Clotet A, Illas F (2001) J Chem Phys 115: 454
25. Payne MC, Peter MP, Allan DC, Arias TA, Joannopoulos JD (1992) Rev Mod Phys 64: 1045
26. Ruette F, Gonzalez C, Octavio A (2001) THEOCHEM 537: 17
27. Ruette F (ed) (1992) Quantum chemistry approaches to chemisorption and heterogeneous catalysis. Kluwer, Dordtrecht
28. Sorescu DC, Yates JT (1998) J Phys Chem B 102: 4556
29. Yang Z, Wu R, Zhang Q, Goodman DW (2001) Phys Rev B 63: 045419
30. Rodriguez JA, Jirsak T, Pérez M, González L, Maiti A (2001) J Chem Phys 114: 4186
31. Rodriguez JA, Jirsak T, Chaturvedi S (1999) J Chem Phys 111:8077
32. Pacchioni G, Rösch N (1996) J Chem Phys 104: 7329
33. Sousa C, Illas F, Bo C, Poblet JM (1993) Chem Phys Lett 215: 97
34. Albaret T, Finocchi F, Noguera C (1999) Faraday Discuss 114: 285
35. Rodriguez JA, Hrbek J, Dvorak J, Jirsak T, Maiti A (2001) Chem Phys Lett 336: 377
36. Wichtendahl R, Rodriguez-Rodrigo M, Härtel U, Kuhlenbeck H, Freund HJ (1999) Phys Status Solidi A 173: 93
37. Furuyama S, Fujii H, Kawamura M, Morimoto T (1978) J Phys Chem 82: 1028
38. Nygren M, Pettersson LGM, Barandiaran Z, Seijo L (1994) J Chem Phys 100: 2010
39. Pacchioni G, Neyman KM, Rösch N (1994) J Electron Spectrosc Relat Phenom 69: 13
40. Yudanov IV, Nasluzov VA, Neyman KM, Rösch N (1997) Int J Quantum Chem 65: 975
41. Nygren MA, Pettersson LGM (1996) J Chem Phys 105: 9339
42. Chen L, Wu R, Kioussis N, Zhang Q (1998) Chem Phys Lett 290: 255
43. Pacchioni G (2000) Surf Rev Lett 7: 277
44. Casarin M, Maccato C, Vittadini A (1998) J Phys Chem B 102: 10752
45. Shustorovich E, Baetzold RC (1985) Science 227: 876
46. Hoffman R (1988) Solids and surfaces: A chemist's view of bonding in extended surfaces. VCH, New York
47. Hammer B, Morikawa Y, Nørskov JK (1996) Phys Rev Lett 76: 2141
48. Sorescu DC, Rusu CN, Yates JT (2000) J Phys Chem B 104: 4408
49. Rodriguez JA, Jirsak T, Liu G, Hrbek J, Dvorak J, Maiti A (2001) J Am Chem Soc 123: 9597
50. Soave R, Pacchioni G (2000) Chem Phys Lett 320: 345
51. Sayle TXT, Parker SC, Catlow CRA (1994) Surf Sci 316: 329
52. Liu G, Rodriguez JA, Hrbek J, Dvorak J, Peden CHF (2001) J Phys Chem B 105: 7762
53. Rodriguez JA, Hrbek J (1999) Acc Chem Res 32: 719
54. Rodriguez JA (2001) Ciencia 9: 139
55. Rodriguez JA, Chaturvedi S, Kuhn M, Hrbek J (1998) J Phys Chem B 102:5 511
56. Rodriguez JA, Chaturvedi S, Kuhn M (1998) Surf Sci Lett 415: L1065
57. Parr RG, Yang W (1989) Density-functional theory of atoms and molecules. Oxford University Press, New York
58. Satterfield CN (1980) Heterogeneous catalysis in practice. McGraw-Hill, New York
59. Kolamakov A, Stultz J, Goodman DW (2000) J Chem Phys 113: 7564
60. Yakshinskiy BV, Madey TE (1999) Nature 400: 642
61. Rodriguez JA, Kuhn M, Hrbek J (1996) J Phys Chem 100: 18240
62. Moeller T (1982) Inorganic chemistry: a modern introduction. Wiley, New York
63. Leysen R, Hopkins BJ, Taylor PA (1975) J Phys C Solid State Phys 8: 907
64. Rodriguez JA, Jirsak T, Hrbek J (1999) J Phys Chem B 103: 1966
65. Snyder JA, Jaffe JE, Gutowski M, Lin Z, Hess AC (2000) J Chem Phys 112: 3014
66. Rodriguez JA, Perez M, Jirsak T, Gonzalez L, Maiti A (2001) Surf Sci 477: L279
67. Bredow T, Apra E, Catti M, Pacchioni G (1998) Surf Sci 418: 150
68. Bredow T (1999) Int J Quantum Chem 75: 127
69. Calzado CJ, San Miguel MA, Sanz JF (1999) J Phys Chem B 103: 480
70. Onishi H, Egawa C, Aruga T, Iwasawa Y (1987) Surf Sci 191: 479
71. Heise R, Courths R (1995) Surf Sci 331–333: 1460
72. Nerlov J, Christensen SV, Wichel S, Pedersen EH, Møller P (1997) Surf Sci 371: 321
73. Rodriguez JA, Jirsak T, Chaturvedi S, Hrbek J (1998) Surf Sci 407: 171
74. Snyder JA, Jaffe JE, Lin Z, Hess AC, Gutowski M (2000) Surf Sci 445: 495
75. Jirsak T, Dvorak J, Rodriguez JA (1999) J Phys Chem B 103: 5550
76. Pacchioni G, Clotet A, Ricart JM (1994) Surf Sci 315: 337
77. Rodriguez JA, Jirsak T, Freitag A, Larese J, Maiti A (2000) J Phys Chem B 104: 7439

78. Schneider WF, Li J, Hass KC (2001) J Phys Chem B 105: 6972
79. Wells AF (1987) Structural inorganic chemistry, 6th edn. Oxford University Press, New York
80. Cockayne B, Jones DW (eds) (1972) Modern cxide materials. Academic, New York.
81. Rodriguez JA, Hanson JC, Chaturvedi S, Maiti A, Brito JL (2000) J Chem Phys 112: 935
82. de Carolis S, Pascual JL, Petterson LGM, Baudin M, Wójcik M, Hermansson K, Palmqvist AEC, Muhammed M (1999) J Phys Chem B 103: 7627
83. Rodriguez JA, Hanson JC, Chaturvedi S, Maiti A, Brito JL (2000) J Phys Chem B 104: 8145
84. Goniakowski J, Noguera C (1996) Surf Sci 365: 1657
85. Pojani A, Finocchi F, Noguera C (1999) Surf Sci 442: 179
86. Cora F, Catlow CRA (1999) Faraday Discuss 114: 421
87. Meyer B, Padilla J, Vanderbilt D (1999) Faraday Discuss 114: 395
88. Matveev AV, Neyman KM, Yudanov IV, Rösch N (1999) Surf Sci 426: 123
89. Sleight AW, Chamberland BL (1968) Inorg Chem 7: 1672
90. Abrahams SC, Reddy JM (1965) J Chem Phys 43: 2533
91. Brito JL, Barbosa AL (1997) J Catal 171: 467
92. Madeira LM, Portela MF, Mazzochia C, Kaddouri A, Anouchinsky R (1998) Catal Today 40: 229
93. Miller J, Sault AG, Jackson NB, Evans L, Gonzalez MM (1999) Catal Lett 58: 147
94. Brito JL, Laine J, Pratt KC (1989) J Mater Sci 24: 425
95. Rodriguez JA, Chaturvedi S, Hanson JC, Brito JL (1999) J Phys Chem B 103: 770
96. Tomishige K, Chen Y, Fujimoto K (1999) J Catal 181: 91
97. Kale GM (1991) J Am Ceram Soc 74:2209
98. Nagaoka K, Karasuda T, Aika K (1999) J Catal 181: 160
99. Lunsford JH (1990) Catal Today 6: 235
100. Chen Y, Tomishige K, Yokoyama K, Fujimoto K (1997) Appl Catal A 165: 335
101. Rodriguez J, Pérez M, Jirsak, T, González L, Maiti A, Larese JZ (2001) J Phys Chem B 105: 5497
102. Rodriguez JA, Jirsak T, Pérez M, Chaturvedi S, Kuhn M, González L, Maiti A (2000) J Am Chem Soc 122: 12362
103. Rodriguez JA, Jirsak T, González L, Evans J, Pérez M, Maiti A (2001) J Chem Phys 115: 10914
104. Rodriguez JA (1990) Surf Sci 226:101
105. Rochefort A, Fournier R (1996) J Phys Chem 100: 13506
106. Illas F, López N, Ricart JM, Clotet A, Conesa JC, Fernández-García M (1998) J Phys Chem B 102: 8017
107. Mamontov E, Egami T, Brezny R, Koranne M, Tyagi S (2000) J Phys Chem B 104: 11110
108. Baxter R, Reinhardt P, Lopez N, Illas F (2000) Surf Sci 445: 448
109. Wang XG, Chaka A, Scheffler M (2000) Phys Rev Lett 84: 3650